Manganese-Enhanced Magnetic Resonance Imaging Detects Declining Pancreatic β-Cell Mass in a Cyclophosphamide-Accelerated Mouse Model of Type 1 Diabetes

Patrick F. Antkowiak,[1] Brian K. Stevens,[2] Craig S. Nunemaker,[3] Marcia McDuffie,[2,3] and Frederick H. Epstein[1,4]

Currently, there is no ideal noninvasive method to quantify the progressive loss of pancreatic β-cell mass (BCM) that occurs in type 1 diabetes. Magnetic resonance imaging has detected gross differences in BCM between healthy and diabetic mice using the contrast agent manganese, which labels functional β-cells and increases the water proton relaxation rate (R1), but its ability to measure gradations in BCM during disease progression is unknown. Our objective was to test the hypothesis that measurements of the manganese-enhanced pancreatic R1 could detect decreasing BCM in a mouse model of type 1 diabetes. We used cyclophosphamide-accelerated BDC2.5 T-cell receptor transgenic nonobese diabetic mice, which experience development of type 1 diabetes during a 7-day time period after cyclophosphamide injection, whereas transgene-negative mice do not. We measured the manganese-enhanced pancreatic R1 before cyclophosphamide injection (day 0) and on days 3, 4, 5, and 7 afterward. Pancreatic R1 remained constant in transgene-negative mice and decreased stepwise day-to-day in transgene-positive mice, mirroring their loss of BCM, confirmed by pancreatic insulin measurements and histology. Changes in R1 in transgene-positive mice occurred before elevations in blood glucose, a clinical indicator of diabetes, suggesting potential for early noninvasive detection of changes in functional BCM. ***Diabetes*** **62:44–48, 2013**

Type 1 diabetes is a metabolic disorder characterized by an inability to maintain normoglycemia. It occurs due to the autoimmune destruction of the insulin-producing pancreatic β-cells, which are diffusely dispersed throughout the pancreas in the islets of Langerhans and represent approximately 1–2% of the pancreatic mass (1). The etiology of this destructive autoimmune process remains largely unknown, although key cellular events include early functional disruption and progressive inflammatory β-cell destruction (2–4). Currently, there is no ideal method for noninvasively measuring changes in functional β-cell mass (BCM), which would be valuable for assessing diabetes progression, following therapeutic response, or for evaluating the viability of transplanted pancreatic islets (5). Provocative testing with β-cell secretogogues, the gold standard for detection of β-cell loss, is insensitive to early stages of the disease, and although biopsy techniques might be useful in monitoring the status of clustered transplanted islets in defined sites, this approach is impractical for dispersed islet transfers or in the diagnosis and staging of type 1 diabetes.

Recently, noninvasive imaging techniques such as single photon emission computed tomography (SPECT) (6), positron emission tomography (7,8), bioluminescence imaging (9), and magnetic resonance imaging (MRI) (10–13) have shown promise in detecting BCM. These techniques, however, have limitations. Positron emission tomography and single photon emission computed tomography use ionizing radiation, have relatively low spatial resolution, and currently use non-ideal β-cell–specific radiotracers; bioluminescence imaging has limited spatial resolution and is not translatable to humans; and no technique has proven the ability to detect small gradations in BCM. Manganese (Mn^{2+})-enhanced MRI (MEMRI) may prove an attractive method for assessing functional BCM, because the mechanism by which Mn^{2+} ions label β-cells is inherently linked to β-cell function and may be translatable to human imaging. Manganese ions enter β-cells through voltage-gated calcium channels (10) and increase the nuclear magnetic resonance water proton longitudinal relaxation rate constant (R1) proportionally with Mn^{2+} concentration. Recent data supporting this mechanism showed that glucose stimulation before MEMRI increased pancreatic R1, and that this effect is essentially abolished with calcium channel blockade (12). Thus, the glucose-stimulated Mn^{2+}-enhanced pancreatic R1 has been interpreted as a measurement of functional BCM (12). MEMRI studies previously have detected gross decreases in BCM in mice in a streptozotocin-induced model of type 1 diabetes (11–13), a model characterized by a precipitous loss of BCM after streptozotocin injection. The sensitivity of MEMRI, or any other imaging modality, to detect gradual changes in functional BCM that occur during the progression of diabetes has not yet been demonstrated, although the ability to measure gradations in BCM is necessary for clinical translation of any technique that assesses functional BCM.

To test the hypothesis that MEMRI can detect gradations in BCM, we performed MRI on cyclophosphamide-accelerated BDC2.5 T-cell receptor transgenic mice on a nonobese diabetic background (NOD-BDC2.5) (14–16). After injection of cyclophosphamide, NOD-BDC2.5 mice expressing a transgenic T-cell receptor (Tg^+ mice) exhibit progressive autoimmune β-cell destruction, with virtually 100% of mice becoming

From the [1]Department of Biomedical Engineering, University of Virginia, Charlottesville, Virginia; the [2]Department of Microbiology, Immunology, and Cancer Biology, University of Virginia, Charlottesville, Virginia; the [3]Department of Medicine, University of Virginia, Charlottesville, Virginia; and the [4]Department of Radiology, University of Virginia, Charlottesville, Virginia.
Corresponding author: Frederick H. Epstein, fredepstein@virginia.edu.
Received 9 February 2012 and accepted 7 July 2012.
DOI: 10.2337/db12-0153

overtly diabetic within 7 days of cyclophosphamide injection (14). Mice lacking the transgenic T-cell receptor (Tg^- mice) do not have development of diabetes within this time frame after cyclophosphamide injection. Because of the kinetics and reproducibility of diabetes progression, this model allows the investigation of the ability to detect small decrements in functional BCM.

RESEARCH DESIGN AND METHODS

All animal experiments were performed under protocols approved and monitored by our Institutional Animal Care and Use Committee.

Type 1 diabetes mouse model. To initiate type 1 diabetes progression, 200 mg/kg cyclophosphamide was injected intraperitoneally in 27 Tg^+ NOD-BDC2.5 mice and in 25 Tg^- littermates. Imaging was performed before cyclophosphamide injection on experimental day 0 and on days 3, 4, 5, and 7 after injection during the period of loss of BCM. The number of mice imaged on each experimental day was as follows (Tg^+/Tg^-): 5/5 on day 0; 8/4 on day 3; 4/6 on day 4; 5/5 on day 5; and 5/5 on day 7. Fasting blood glucose was measured before imaging as an indicator of type 1 diabetes using a OneTouch glucose meter (LifeScan). After one imaging session, the complete pancreas was harvested from each mouse for pancreatic insulin measurement.

Imaging protocol. MRI was performed on a 7-Tesla Clinscan system (Bruker, Etlingen, Germany) using a 30-mm inner-diameter mouse whole-body radiofrequency coil. Mice were anesthetized with 1.25% isoflurane. Mice were injected with glucose (1.5 g/kg) to stimulate β-cell Ca^{2+} channels 2 min before injecting $MnCl_2$ (100 μmol/kg) to label β-cells as described (11,12). The pancreas was localized using coronal and axial images (11,12), and the splenic region of the pancreas was imaged. Look-Locker MRI (17) was performed 1 h after glucose and $MnCl_2$ injections to quantify pancreatic R1, a time that was demonstrated to be optimal for imaging Mn^{2+}-enhanced β-cells in a previous study (12). Look-Locker MRI acquires frame-by-frame images of the recovery of longitudinal magnetization toward its equilibrium after magnetization inversion. From these images, which are separated by intervals of the inversion time, the relaxation rate R1 can be accurately quantified pixel-wise. The Look-Locker pulse sequence used a nonselective 180-degree inversion pulse followed by a train of gradient echoes separated by inversion times between 30 and 50 ms. Specific imaging parameters were: time between successive inversions = 5,500 ms; echo time = 1.9 ms; flip angle = 3 degrees; slice thickness = 1 mm; number of slices = 1; field of view = 35 × 25 mm; matrix = 64 × 48; number of images = 100; averages = 3; and 500 μm in-plane resolution.

Image analysis. A region of interest was drawn around the pancreas to generate pancreatic signal intensity versus time curve. This curve was modeled as an exponential relaxation curve of the form $M_z(t) = M_0[1-2*exp(-t*R1)]$, where $M_z(t)$ is the longitudinal magnetization and M_0 is the equilibrium magnetization, and fit for R1 was found using a Marquardt-Levenberg optimization algorithm in MATLAB (Mathworks, Natick, MA). Pixel-wise pancreatic R1 maps were additionally calculated. Statistical testing was performed using two-way ANOVA, and results are reported as mean ± SD.

Pancreatic insulin content. After imaging, mice were killed, and their pancreata were harvested for pancreatic insulin content measurement. The number of pancreata harvested on each experimental day corresponded to the number and type of mice imaged that day. The pancreas was removed, and pancreatic insulin was extracted in ethanol acid (18). The time between glucose administration and pancreatic harvest was 1.5 h and was consistent for all experiments. Total pancreatic insulin concentrations were determined using a mouse insulin enzyme-linked immunosorbent assay (Mercodia Mouse Insulin ELISA Kit, Mercodia AB, Uppsala, Sweden) and quantitated against a standard curve.

Histological scoring. Pancreatic histology was performed as described elsewhere (19). Pancreata were harvested from a parallel cohort of Tg^- (n = 11) and Tg^+ (n = 18) mice on days 3 (4 Tg^-/5 Tg^+), 5 (3 Tg^-/6 Tg^+), and 8 (4 Tg^-/7 Tg^+) after cyclophosphamide administration, since the entire pancreas from each imaged mouse was used to measure pancreatic insulin. The 5-μm pancreatic sections were embedded in paraffin and stained with aldehyde fuchsin, to stain for insulin-positive β-cells, and hematoxylin, to highlight nuclei and areas of mononuclear infiltration. Three sections were scored per mouse. An insulin score was determined as a product of the residual total islet mass, estimated as a fraction of that in age-matched and sex-matched NOD.scid control mice (0.0–1.0) multiplied by the average percentage of aldehyde fuchsin–positive cells per islet relative to control (0–100%). An insulitis score was determined on a 0–3 scale, with scoring as follows: 0, no infiltrate; 1, polar infiltrate only; 2, infiltrating cells extending around islet to >50% of its circumference without invasion; and 3, invasive insulitis.

RESULTS

Pancreatic insulin, blood glucose measurements, and pancreatic histology. Pancreatic insulin content decreased significantly on days 3–7 after cyclophosphamide injection in Tg^+ mice, mirroring their disease progression and loss of BCM, whereas Tg^- mice maintained constant pancreatic insulin during all experimental days (Fig. 1*A*). These observations agree with other studies using this model (14–16). Blood glucose concentration (Fig. 1*B*), a clinical indicator of type 1 diabetes, increased significantly in Tg^+ mice only on day 7 ($P < 0.01$). Thus, the majority of β-cell damage had occurred before the manifestation of increased blood glucose, as has been reported previously (14).

Histology was performed to further assess functional BCM and the extent of pancreatic immune infiltration. Specifically, insulin and insulitis scores were generated from the histological sections. Representative pancreatic histological sections are shown in Fig. 1*C–H* for Tg^- and Tg^+ mice on experimental days 3, 5, and 8. Figure 1*I* confirms that Tg^- mice maintained stable functional BCM during the first 7 days after cyclophosphamide injection, whereas functional BCM decreased in Tg^+ mice from day 3 to day 5. Islet infiltration was prevalent in Tg^+ mice starting at day 3 (Fig. 1*J*) but was not observed in Tg^- mice until day 8.

Mn^{2+}-enhanced pancreatic R1 reflects the progressive decline of BCM in Tg^+ mice. Having characterized the mouse model, our objective was to determine whether MEMRI could accurately measure graded changes in BCM. Figure 2*A* shows example Look-Locker images of the pancreas acquired 1 h after glucose and $MnCl_2$ injections, with the pancreas outlined in red. Typical pancreatic signal intensity versus time curves, normalized by M_0 to be on a −1 to 1 scale, are shown in Fig. 2*B*. The difference between the curves for Tg^+ and Tg^- mice on experimental day 3 is observable, showing a decrease in R1 for the Tg^+ mouse. The pixel-wise pancreatic R1 maps for these two mice are overlain in color on anatomic reference images in Fig. 2*C*.

The measured Mn^{2+}-enhanced pancreatic R1s are shown in Fig. 3*A* for Tg^+ and Tg^- mice on experimental days 0 and 3–7. Pancreatic R1 remained constant after cyclophosphamide injection in Tg^- mice and decreased progressively in Tg^+ mice, mirroring the trends observed in pancreatic insulin (Fig. 1*A*). Two-way ANOVA revealed significant differences in Mn^{2+}-enhanced pancreatic R1 for same-day Tg^+ mice versus Tg^- mice for all days except day 0 ($^*P < 0.01$). Pancreatic R1 for day 0 Tg^+ mice was statistically different from Tg^+ mice on all other experimental days ($P < 0.05$), and pancreatic R1 for day 3 Tg^+ mice was significantly different from that of day 7 Tg^+ mice ($P < 0.05$). Mn^{2+}-enhanced pancreatic R1 correlated well with total pancreatic insulin content, our gold standard measurement of BCM, with an R^2 of 0.76 (Fig. 3*B*). These data provide proof-of-principle that this noninvasive MRI-based approach may be able to detect the early declines in BCM that precede hyperglycemia in type 1 diabetes.

A limitation of this study is that we imaged only a single slice of the pancreas, in the splenic region. We imaged the splenic region of the pancreas to achieve consistency between imaging studies, because this region is readily identified using anatomic landmarks (11,12). In mice, there is no consensus evidence for the preferential distribution of islets by pancreatic region, and histology showed similar cellular infiltration throughout the pancreas. Therefore, we posit that the splenic region is representative of the

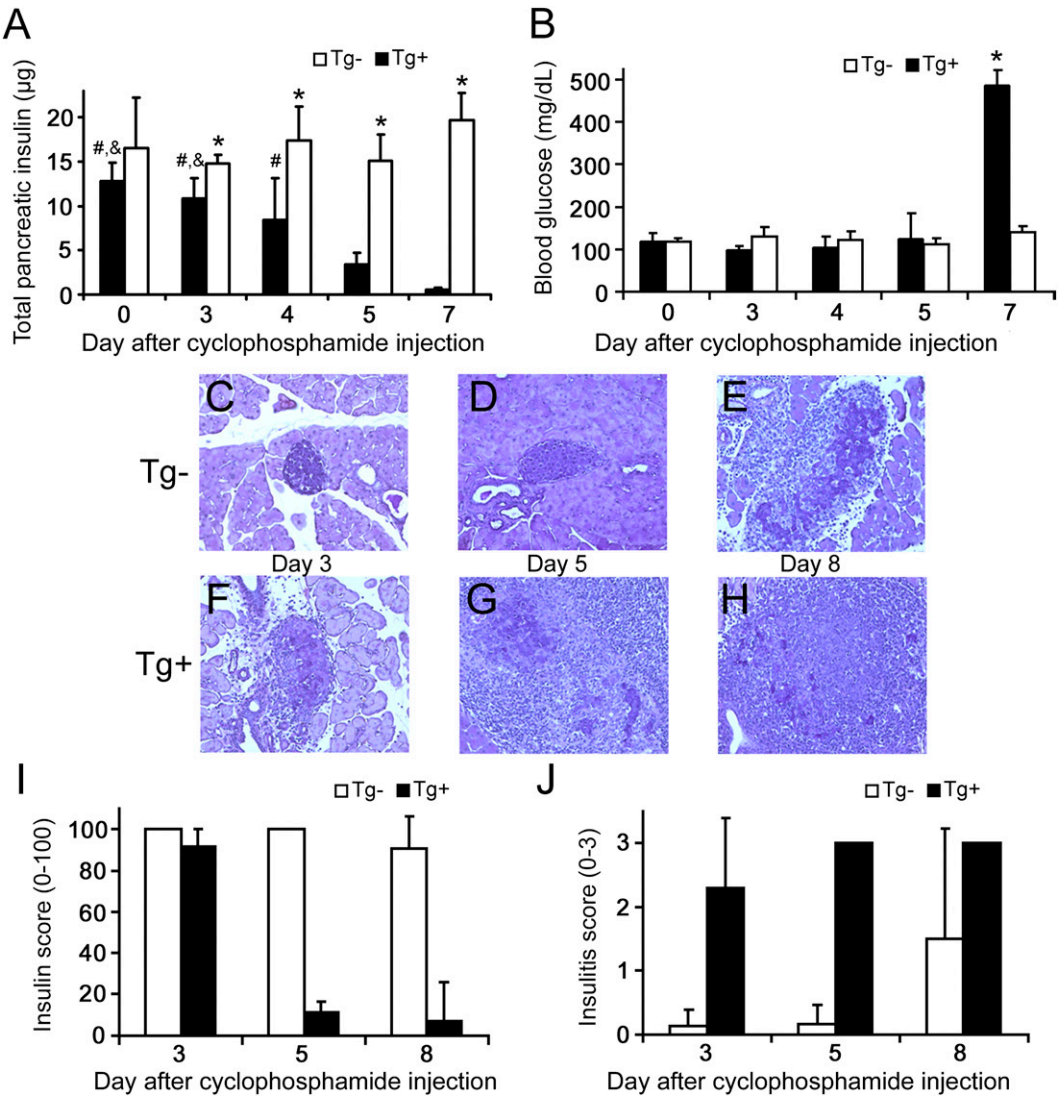

FIG. 1. Characteristics of the cyclophosphamide-injected mouse model of type 1 diabetes. White bars, Tg^- mice; black bars, Tg^+ mice. All data are presented as mean ± SD. *A*: Total pancreatic insulin indicated the loss of BCM in Tg^+ mice during the experimental time course (*$P < 0.05$ vs. same-day Tg^+; &$P < 0.01$ vs. day 5 Tg^+; #$P < 0.01$ vs. day 7 Tg+), whereas BCM remained constant after cyclophosphamide injection in Tg^- mice. *B*: The decreased BCM in Tg^+ mice was registered as an increase in blood glucose only after day 7, by which time loss of BCM had already occurred. *C–H*: Histological changes in cyclophosphamide-treated mice. Five-micron sections were stained with aldehyde fuchsin (deep violet) to visualize β-cell insulin granules; a hematoxylin counterstain (light blue) was used to identify nuclei and highlight areas of mononuclear infiltration. Representative sections are shown at ×200 magnification. *C* and *D*: Pancreatic infiltration was minimal before day 5 in nontransgenic mice, whereas invasive insulitis with some evidence of β-cell damage had developed by day 8 in some of these mice (*E*). In contrast, invasive insulitis was clearly evident by day 3 in Tg^+ mice (*F*), with increasing evidence of destructive insulitis in all mice by day 5 (*G*). In the single mouse remaining nondiabetic by day 8, extensive islet damage was widespread, with only small numbers of residual β-cells retaining detectable insulin granules (*H*). No granulated β-cells were seen in sections from diabetic mice (not shown). *I*: Histological insulin score, indicative of BCM, decreased in Tg^+ mice but remained relatively constant in Tg^- mice. *J*: Histological insulitis score on a 0–3 scale.

entire mouse pancreas. To overcome this limitation, a multislice Look-Locker imaging method may be implemented in the future.

Another potential limitation is nonspecific uptake of Mn^{2+} by other cells, which could potentially affect the ability of MEMRI to detect β-cell pathophysiology. To address this possibility, we have previously investigated the effects of nonspecific Mn^{2+} uptake on pancreatic R1 and found that using Mn^{2+} enhancement after glucose stimulation provides β-cell specificity (12). A further limitation of this study is that changes in vascularity associated with diabetes progression that could potentially alter Mn^{2+} uptake in the pancreas were not accounted for in our analysis.

Safety is a concern with the use of unchelated $MnCl_2$ in humans. Although in vitro (10) and small animal studies report no functional impairment of β-cell insulin secretion by Mn^{2+}, systemic effects such as elevated heart rate and blood pressure were observed in dogs with a $MnCl_2$ dose of 30 μmol/kg (20). The use of $MnCl_2$ recently has been explored in humans (21); however, at a dose of 5 μmol/kg (1/20th the dose used in this study), with no adverse effects. More promising is the use of the chelated Mn^{2+}-based agent Teslascan (GE Healthcare), which is approved for imaging the human liver and has been shown to assess the function of other tissues in rodents (22). Another Mn^{2+}-based agent, EVP-1001 (Eagle Vision Pharmaceuticals), is in phase II clinical trials and has been used to measure myocyte function after myocardial infarction (23). The use of lower $MnCl_2$ doses or approved Mn^{2+}-based contrast agents will be explored in the future to allow potential clinical translation of

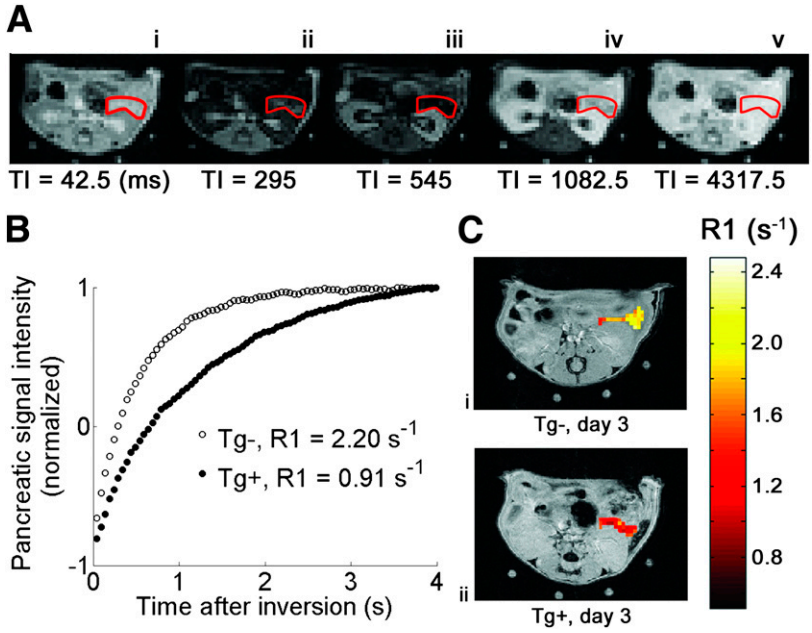

FIG. 2. *A*: A series of Look-Locker images showing an axial slice through the mouse abdomen, with the pancreas outlined in red. After inversion at time 0, longitudinal magnetization returns to equilibrium with relaxation rate constant R1. The specific time after inversion (TI, in ms) is indicated below each image. *B*: Example pancreatic signal intensity vs. time curves for a Tg^- (white circles) mouse and Tg^+ (black circles) mouse on day 3 after cyclophosphamide injection. Each data point on the curves represents the normalized pancreatic signal intensity measured at one TI. Pancreatic R1 was calculated by applying a monoexponential recovery model to each curve. *C*: Pixel-wise R1 maps of the pancreas from Tg^- (*i*) and Tg^+ (*ii*) mice on experimental day 3 overlain on high-resolution anatomic reference images. R1 is decreased in the Tg^+ mouse at day 3 after cyclophosphamide injection.

this technique. Finally, clinical translation will require rapid R1 mapping methods capable of imaging the entire pancreas with high spatial resolution, such as modified Look-Locker imaging (24), the standard method for R1 mapping in the heart. Compressed sensing (25) may allow the development of improved methods for rapid pancreatic R1 mapping in the future.

In conclusion, measurements of pancreatic R1 after glucose stimulation and Mn^{2+} labeling of functional β-cells accurately reflected changes in BCM in this mouse model of type 1 diabetes, as pancreatic R1 correlated well with both pancreatic insulin content and histological estimates of BCM. Significant decreases in pancreatic R1 were observed in Tg^+ mice not only from day 0 to day 7, at which time the mice had frank diabetes, but also from days 3 to 5, while β-cell damage occurred during the progression to diabetes. Importantly, MRI measured these decreases before blood glucose increased, indicating that the technique may have the sensitivity to detect decreases in BCM that occur before onset of clinical type 1 diabetes (26,27). The ability to detect the loss of BCM during this time is paramount, because this may be the critical period in which to salvage BCM (28).

ACKNOWLEDGMENTS

This study was supported by the American Diabetes Association Basic Science Award, Grant 7-09-BS-52, and by a Univeristy of Virginia LaunchPad award.

No potential conflicts of interest relevant to this article were reported.

P.F.A. researched data, contributed to discussion, and wrote the manuscript. B.K.S. researched data. C.S.N. researched data and reviewed and edited the manuscript.

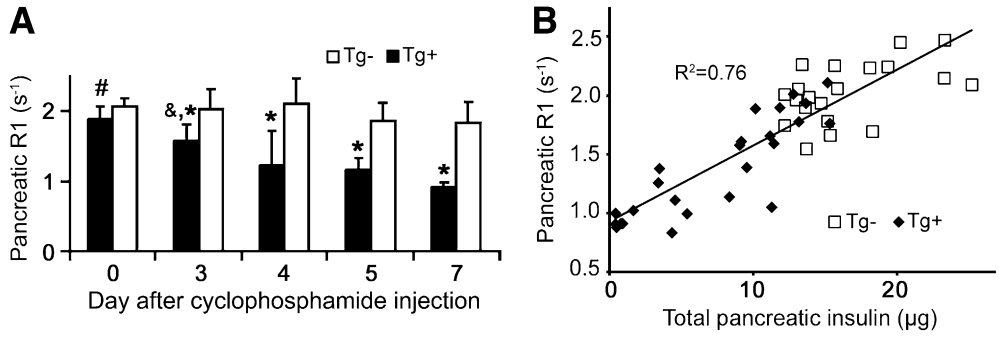

FIG. 3. *A*: The Mn^{2+}-enhanced pancreatic R1 reflected the changes seen in pancreatic insulin content, with pancreatic R1 remaining constant in Tg^- mice (white bars) and declining progressively in Tg^+ mice (*$P < 0.01$ vs. same-day Tg^+, #$P < 0.05$ vs. all other Tg^+, &$P < 0.05$ vs. day 7 Tg^+) after cyclophosphamide injection. White bars, Tg^- mice; black bars, Tg^+ mice. *B*: Mn^{2+}-enhanced pancreatic R1 correlated well with total pancreatic insulin, with $R^2 = 0.76$. White squares, Tg^- mice; black diamonds, Tg^+ mice.

M.M. researched data, contributed to discussion, and reviewed and edited the manuscript. F.H.E. contributed to discussion and reviewed and edited the manuscript. F.H.E. is the guarantor of this work and, as such, had full access to all the data in the study and takes responsibility for the integrity of the data and the accuracy of the data analysis.

Parts of this study were presented in abstract form (Abstract 3008) at the 19th Annual Meeting of the International Society for Magnetic Resonance in Medicine, Montreal, Quebec, Canada, 13–17 May 2011.

The authors acknowledge Kathryn L. Corbin, of the University of Virginia Diabetes Research Center Islet Isolation Core, for performing the insulin content measurements.

REFERENCES

1. Ahlgren U, Gotthardt M. Approaches for imaging islets: recent advances and future prospects. Adv Exp Med Biol 2010;654:39–57
2. Eizirik DL, Mandrup-Poulsen T. A choice of death—the signal-transduction of immune-mediated beta-cell apoptosis. Diabetologia 2001;44:2115–2133
3. Meier JJ, Bhushan A, Butler AE, Rizza RA, Butler PC. Sustained beta cell apoptosis in patients with long-standing type 1 diabetes: indirect evidence for islet regeneration? Diabetologia 2005;48:2221–2228
4. Rabinovitch A, Baquerizo H, Pukel C, Sumoski W. Effects of cytokines on rat pancreatic islet cell monolayer cultures: distinction between functional and cytotoxic effects on islet beta-cells. Reg Immunol 1989;2:77–82
5. Shapiro AM, Lakey JR, Ryan EA, et al. Islet transplantation in seven patients with type 1 diabetes mellitus using a glucocorticoid-free immunosuppressive regimen. N Engl J Med 2000;343:230–238
6. Moore A, Bonner-Weir S, Weissleder R. Noninvasive in vivo measurement of beta-cell mass in mouse model of diabetes. Diabetes 2001;50: 2231–2236
7. Simpson NR, Souza F, Witkowski P, et al. Visualizing pancreatic beta-cell mass with [^{11}C]DTBZ. Nucl Med Biol 2006;33:855–864
8. Souza F, Simpson N, Raffo A, et al. Longitudinal noninvasive PET-based beta cell mass estimates in a spontaneous diabetes rat model. J Clin Invest 2006;116:1506–1513
9. Yong J, Rasooly J, Dang H, et al. Multimodality imaging of β-cells in mouse models of type 1 and 2 diabetes. Diabetes 2011;60:1383–1392
10. Gimi B, Leoni L, Oberholzer J, et al. Functional MR microimaging of pancreatic beta-cell activation. Cell Transplant 2006;15:195–203
11. Antkowiak PF, Tersey SA, Carter JD, et al. Noninvasive assessment of pancreatic beta-cell function in vivo with manganese-enhanced magnetic resonance imaging. Am J Physiol Endocrinol Metab 2009;296:E573–E578
12. Antkowiak PF, Vandsburger MH, Epstein FH. Quantitative pancreatic beta cell MRI using manganese-enhanced Look-Locker imaging and two-site water exchange analysis. Magn Reson Med 2012;67:1730–1739
13. Lamprianou S, Immonen R, Nabuurs C, et al. High-resolution magnetic resonance imaging quantitatively detects individual pancreatic islets. Diabetes 2011;60:2853–2860
14. André-Schmutz I, Hindelang C, Benoist C, Mathis D. Cellular and molecular changes accompanying the progression from insulitis to diabetes. Eur J Immunol 1999;29:245–255
15. Yasunami R, Bach JF. Anti-suppressor effect of cyclophosphamide on the development of spontaneous diabetes in NOD mice. Eur J Immunol 1988; 18:481–484
16. Brode S, Raine T, Zaccone P, Cooke A. Cyclophosphamide-induced type-1 diabetes in the NOD mouse is associated with a reduction of CD4+CD25 +Foxp3+ regulatory T cells. J Immunol 2006;177:6603–6612
17. Look DC, Locker DR. Time saving in measurement of NMR and EPR relaxation times. Rev Sci Instrum 1970;41:250–251
18. Amrani A, Durant S, Throsby M, Coulaud J, Dardenne M, Homo-Delarche F. Glucose homeostasis in the nonobese diabetic mouse at the prediabetic stage. Endocrinology 1998;139:1115–1124
19. McDuffie M, Maybee NA, Keller SR, et al. Nonobese diabetic (NOD) mice congenic for a targeted deletion of 12/15-lipoxygenase are protected from autoimmune diabetes. Diabetes 2008;57:199–208
20. Jynge P, Brurok H, Asplund A, Towart R, Refsum H, Karlsson JO. Cardiovascular safety of MnDPDP and MnCl2. Acta Radiol 1997;38:740–749
21. Fernandes JL, Storey P, da Silva JA, de Figueiredo GS, Kalaf JM, Coelho OR. Preliminary assessment of cardiac short term safety and efficacy of manganese chloride for cardiovascular magnetic resonance in humans. J Cardiovasc Magn Reson 2011;13:6
22. Tofts PS, Porchia A, Jin Y, Roberts R, Berkowitz BA. Toward clinical application of manganese-enhanced MRI of retinal function. Brain Res Bull 2010;81:333–338
23. Storey P, Chen Q, Li W, et al. Magnetic resonance imaging of myocardial infarction using a manganese-based contrast agent (EVP 1001-1): preliminary results in a dog model. J Magn Reson Imaging 2006;23:228–234
24. Messroghli DR, Radjenovic A, Kozerke S, Higgins DM, Sivananthan MU, Ridgway JP. Modified Look-Locker inversion recovery (MOLLI) for high-resolution T1 mapping of the heart. Magn Reson Med 2004;52:141–146
25. Lustig M, Donoho D, Pauly JM. Sparse MRI: The application of compressed sensing for rapid MR imaging. Magn Reson Med 2007;58:1182–1195
26. Akirav E, Kushner JA, Herold KC. Beta-cell mass and type 1 diabetes: going, going, gone? Diabetes 2008;57:2883–2888
27. Ziegler AG, Ziegler R, Vardi P, Jackson RA, Soeldner JS, Eisenbarth GS. Life-table analysis of progression to diabetes of anti-insulin autoantibody-positive relatives of individuals with type I diabetes. Diabetes 1989;38: 1320–1325
28. Atkinson MA, Eisenbarth GS. Type 1 diabetes: new perspectives on disease pathogenesis and treatment. Lancet 2001;358:221–229